International Journal of Nanomedicine

Dovepress
open access to scientific and medical research

Open Access Full Text Article

ORIGINAL RESEARCH

p66shc siRNA Nanoparticles Ameliorate Chondrocytic Mitochondrial Dysfunction in Osteoarthritis

This article was published in the following Dove Press journal:
International Journal of Nanomedicine

Hyo Jung Shin,[1,2] Hyewon Park,[1,2] Nara Shin,[1,2] Juhee Shin,[1,2] Do Hyeong Gwon,[1,2] Hyeok Hee Kwon,[1,3] Yuhua Yin,[1,2] Jeong-Ah Hwang,[1,2] Jinpyo Hong,[2] Jun Young Heo,[1,4,5] Cuk-Seong Kim,[1,6] Yongbum Joo,[7] Youngmo Kim,[7] Jinhyun Kim,[8] Jaewon Beom,[9] Dong Woon Kim[1,2]

[1]Department of Medical Science, Chungnam National University College of Medicine, Daejeon 35015, Republic of Korea; [2]Department of Anatomy and Cell Biology, Brain Research Institute, Chungnam National University College of Medicine, Daejeon 35015, Republic of Korea; [3]Department of Pediatrics, [4]Biochemistry, [5]Infection Control Convergence Research Center, [6]Physiology Chungnam National University College of Medicine, Daejeon, Republic of Korea; [7]Department of Orthopedics, Chungnam National University College of Medicine, Daejeon, Republic of Korea; [8]Division of Rheumatology, Department of Internal Medicine, Chungnam National University College of Medicine, Daejeon, Republic of Korea; [9]Department of Rehabilitation Medicine, Seoul National University Bundang Hospital, Seongnam, Gyeonggi-do, Republic of Korea

Correspondence: Dong Woon Kim DVM., PhD.
Department of Anatomy and Cell Biology, Chungnam National University College of Medicine, 266 Munhwa-Ro, Chung-Gu, Daejeon 35015, Republic of Korea
Tel +82-42-580-8201
Fax +82-42-586-4800
Email visnu528@cnu.ac.kr

Jinhyun Kim, MD., PhD.
Department of Internal Medicine, Chungnam National University College of Medicine, 266 Munhwa-Ro, Chung-Gu, Daejeon 35015, Republic of Korea
Tel +82-42-338-2420
Fax +82-42-586-4800
Email jkim@cnuh.co.kr

Background: Osteoarthritis (OA) is the most common type of joint disease associated with cartilage breakdown. However, the role played by mitochondrial dysfunction in OA remains inadequately understood. Therefore, we investigated the role played by p66shc during oxidative damage and mitochondrial dysfunction in OA and the effects of p66shc down-regulation on OA progression.

Methods: Monosodium iodoacetate (MIA), which is commonly used to generate OA animal models, inhibits glycolysis and biosynthetic processes in chondrocytes, eventually causing cell death. To observe the effects of MIA and poly(lactic-*co*-glycolic acid) (PLGA)-based nanoparticles, histological analysis, immunohistochemistry, micro-CT, mechanical paw withdrawal thresholds, quantitative PCR, and measurement of oxygen consumption rate and extracellular acidification rate were conducted.

Results: p-p66shc was highly expressed in cartilage from OA patients and rats with MIA-induced OA. MIA caused mitochondrial dysfunction and reactive oxygen species (ROS) production, and the inhibition of p66shc phosphorylation attenuated MIA-induced ROS production in human chondrocytes. Inhibition of p66shc by PLGA-based nanoparticles-delivered siRNA ameliorated pain behavior, cartilage damage, and inflammatory cytokine production in the knee joints of MIA-induced OA rats.

Conclusion: p66shc is involved in cartilage degeneration in OA. By delivering p66shc-siRNA-loaded nanoparticles into the knee joints with OA, mitochondrial dysfunction-induced cartilage damage can be significantly decreased. Thus, p66shc siRNA PLGA nanoparticles may be a promising option for the treatment of OA.

Keywords: osteoarthritis, monosodium iodoacetate, p66shc, ROS, mitochondrial dysfunction, PLGA-based nanoparticles

Introduction

Osteoarthritis (OA), a degenerative joint disease, is the most common type of arthritis associated with cartilage breakdown.[1] OA is a chronic disease characterized by pain, local tissue damage, and attempted tissue repair. Given the increase in life expectancies worldwide, OA has become one of the most common chronic diseases. OA affects various tissues and is associated with articular chondrocyte degeneration and clustering, synovial inflammation, osteophyte formation, and subchondral bone remodeling.[2–4] However, cartilage loss is the primary pathogenic feature of OA,[5] and it is well-known that reactive oxygen species (ROS) play an important role in cartilage degradation and chondrocytes death.[6,7] Patients with OA exhibit different degrees of oxidative stress

and cartilage destruction.[8] In addition, mitochondria has a significant role in cellular functions and cell survival in many degenerative diseases; mitochondrial dysfunction caused by oxidative stress has also been associated with cartilage damage.[9–11]

Recently, p66shc, an isoform of the shcA adaptor protein family, has been shown to play a crucial role in the generation of mitochondrial ROS (mtROS) due to the presence of an additional CH2 domain at the N terminus, which contains a critical serine at position 36 (Ser36); this domain is absent in the other two isoforms, p52Shc and p47Shc.[12] p66shc-knockout mice express reduced intracellular ROS levels.[13] In addition, p66shc phosphorylation has been associated with mitochondrial dysfunction,[14,15] and p66shc-induced oxidative stress may play a role in apoptosis.[13] p66shc has been associated with oxidative stress in kidney, cardiovascular, and lung disease.[16–19] However, the role played by p66shc during articular cartilage degeneration has not been investigated although chondrocytes exhibit reduced mitochondrial membrane potential.[20]

Meanwhile, siRNA-loaded nanoparticles (NPs) for drug delivery in various diseases has been in the spotlight recently.[21–24] Especially, the poly(lactic-*co*-glycolic acid) (PLGA)-based NPs is one of the most effective and commonly used biodegradable polymeric NPs approved by the US FDA. The in-vivo safety of PLGA nanoparticles was well proven in a previous study with SD rats.[25] The single emulsion process (oil-in-water method) is used for water-insoluble drugs such as steroids, whereas the double emulsion (water-in-oil-in-water method) is best suited to encapsulate water-soluble drugs, like peptides, proteins and vaccines. The particle size and encapsulation efficiency of the double emulsion is controlled by choice of solvent and stirring rate.[26,27] There are various factors such as composition, crystallinity, molecular weight, pH, chemical properties of the drug, size and shape of the matrix, and drug loading that affect biodegradation of PLGA.[26] A gene therapy system with the intra-articular administration of p66shc-siRNA-loaded PLGA NPs can be a feasible tool for OA treatment. Thus, we first explored the role played by p66shc during oxidative damage and mitochondrial dysfunction in OA, and the effects of p66shc down-regulation on OA progression.

Materials and Methods

Ethics Approval

All animal-related procedures were conducted in accordance with the guidelines of the Institutional Animal Care and Use Committee of Chungnam National University Hospital (CNUH-017-P0019, CNUH-017-A0028). The Institutional Review Board of Chungnam National University Hospital approved the use of human tissues, and written informed consent was obtained from all patients before the operative procedure (CNUH-2016-06-007).

Animals and Arthritis Models

Male Sprague–Dawley rats weighing 120–140 g at the time of OA induction were used. Under brief isoflurane anesthesia, the animals were intra-articularly injected in the left knee with 0.5, 1, or 2 mg of monosodium iodoacetate (MIA; catalog no. I2512; Sigma-Aldrich, USA) dissolved in 20 μL saline; controls received saline only (day 0).

Histological Analysis and Immunohistochemistry

Tissues fixed in 4% (v/v) paraformaldehyde for 2 days, decalcified in Calci-Clear solution (catalog no. HS-105; National Diagnostics, USA) for 2 days, sectioned in the coronal plane (thickness 4 μm), embedded in paraffin wax and used to prepare slides after staining with hematoxylin. Also, sections were stained with Fast Green (catalog no. 2353-45-9; Daejung, Korea) and Safranin-O (catalog no. CI-50240; Junsei Chemical Co., Korea) to evaluate the extent of histopathological lesions. For immunohistochemistry, antibodies were purchased from the following sources: anti-p-p66shc (Enzo, Alx-804-358), anti-total-shc (BD, 610878). Primary chondrocyte cells were incubated with 3 μM of solution and DAPI for 5 min at RT. Immunofluorescent images were taken on an Axiophot microscope (Carl Zeiss, Germany). To determine cell viability, assay reagent (EZ-Cytox) was purchased from Daeillab Service. Immunostaining was visualized with diaminobenzidine (DAB), and specimens were mounted using Polymount. We used the Image J (National Institute of Health, USA) to assess the immunohistochemical signals quantitatively with densitometric measurements.

Micro-CT

Animal knee joints were subjected to quantitative micro-computed tomography (micro-CT) (Quantum FX, Perkin Elmer, USA) using an X-ray source operating at 90 kV/160 μA and a scan time of 180 s, affording a resolution of 20 μm. We generated cross-sectional slices and reconstructed the joint using threshold values of 0–0.14 to distinguish bone using the Feldkamp back projection algorithm.[28]

Chondrocytes Isolation and Culture

We used a scalpel to excise cartilage from the femoral condyles and tibial condyles of OA patients treated at Chungnam National University Hospital. The cartilage was cut into 2-mm thick pieces and the digested suspension passed through a 40-μM-pore-size cell strainer to isolate individual chondrocytes. Cells (5 X 10^6) were seeded into 10-mm-diameter dishes and cultured for 10 days in Dulbecco's minimal essential medium supplemented with 10% (v/v) fetal bovine serum. The medium was changed every 2 days.[29]

Behavioral Testing

Mechanical paw withdrawal thresholds were measured via up-down Von Frey testing.[30] The number of paw withdrawal responses to normally innocuous mechanical stimuli was measured by using a von Frey filament (North Coast Medical, Morgan Hill, CA). Rats were placed on a metal mesh grid under a plastic chamber, and the von Frey filament was applied from underneath the metal mesh flooring to each hind paw. The von Frey filament was applied 10 times to each hind paw, and the number of paw withdrawal responses out of 10 was then counted. The results of the mechanical behavioral testing for each experimental animal were expressed as a percent withdrawal response frequency (PWF), which represented the percentage of paw withdrawals out of the maximum of 10, as previously described. The CatWalk system measures the mean intensity of the paw print area and the standing phase, which, together, reflect mechanical allodynia and neuropathic pain.[31] CatWalk gait analysis was performed on day 21. The animals traversed a walkway with a glass floor located in a darkened room. In general, rats cross the CatWalk runway easily and at a constant speed. The CatWalk gait analysis system consists of a glass walkway under white fluorescent light. The light rays exhibit complete internal reflection. When an object touches the glass runway, the light is reflected downwards and is detected by a video camera. The signal is digitized and analyzed by dedicated software (CatWalk XT ver. 10.5.505, Noldus, USA).

Quantitative Polymerase Chain Reaction

Total RNAs from primary chondrocytes were isolated using TRIzol Reagent according to the manufacturer's protocol (Gene All, RoboEx^{TM}). The RNA concentration was quantified using Nanodrop spectrometer (Thermo scientific). cDNA was prepared from total RNA using the Kit (enzynomics, B201). Quantitative polymerase chain reaction (qPCR) was performed using the AriaMax Real-time PCR system (Agilent technologies) with the Top real ^{TM} qPCR 2X premix (SYBR Green with low ROX). The primers used for rat TNF-α, IL-1β and COX2 were as follows: rTNF-α 5′-AGATGTGGAACTG GCAGAGG-3′, and antisense 5′-CCCATTTGGGAACTT CTCCT-3′; rIL-1β, 5′-CAGCAGCATCTCGACAAGAG-3′, and antisense 5′-CATCATCCCACGAGTCACAG-3′; rCO X2 5′-CAGTATCAGAACCGCATTGCC-3′, and antisense 5′-GAGCAAGTCCGTGTTCAAGGA-3′.

Adenoviral Infection

Recombinant adenovirus encoding shRNA targeting p66shc was generated using the AdEasy system, as described previously.[17] Primary chondrocytes were infected with adenovirus at a multiplicity of infection (MOI) of 100 in 6-well culture plates. After 48 h, mitochondrial ROS levels were determined by mitoSOX staining (Molecular probes, M36008). Adenovirus with β-galactosidase (Ad-gal), encoding an inert LacZ gene, served as a control virus.

Poly(Lactic-*co*-Glycolic Acid) Nanoparticles Preparation

PLGA NPs with 50:50 ratio of lactic and glycolic acid carrying p66shc siRNA (catalog no. RSS373234; Thermo Fisher, USA) or scrambled siRNA (catalog no. 12935400; Thermo Fisher) were prepared using an emulsification/solvent evaporation method[32] and their physical characteristics were analyzed with the Zetasizer Nano ZS90 (Malvern Instruments, UK).[23] The NP synthesis and characterization are shown in the Figure 1.

Measurement of Oxygen Consumption Rate and Extracellular Acidification Rate

Measurement of oxygen consumption rate (OCR) and extracellular acidification rate (ECAR) were measured using a Seahorse XF-24 analyzer (Seahorse Bioscience, USA). The day before OCR measurement, the sensor cartridge was calibrated using buffer at 37°C. Cells were washed twice with XF assay medium (without sodium bicarbonate or phenol red) and incubated in a 37°C incubator for 1 h prior to calibration. Three readings were taken after addition of each mitochondrial inhibitor and before injection of other inhibitors. The mitochondrial inhibitors used were oligomycin (2 μg/mL), carbonyl cyanide m-chlorophenylhydrazone (CCCP) (5 μM), and rotenone (2 μM). The OCR and ECAR were automatically calculated by the sensor cartridge and the

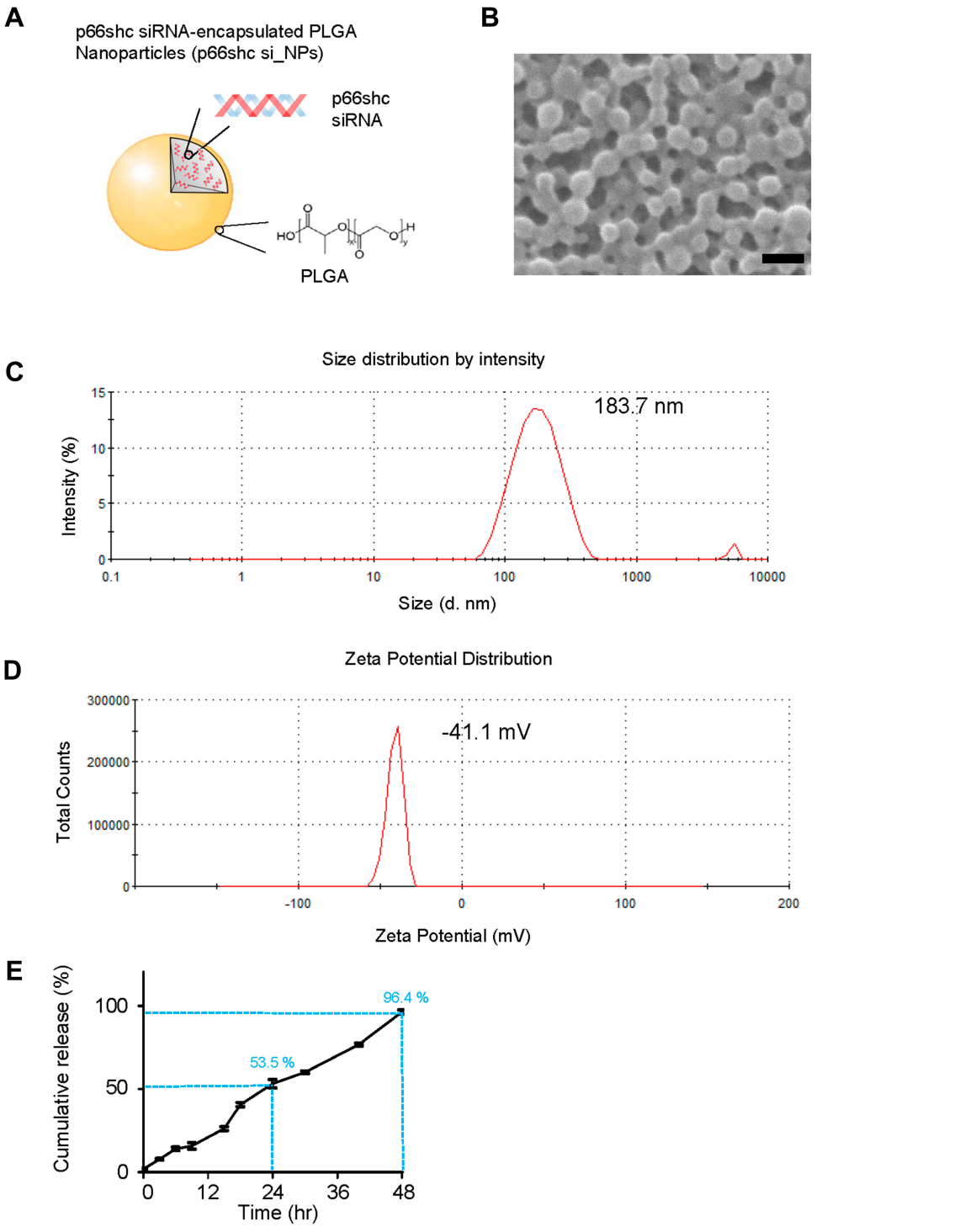

Figure 1 Synthesis and physical characteristics of p66shc siRNA-encapsulated PLGA NPs.

Notes: (**A**) To prepare PLGA nanoparticles, 200 μL of 20 μM siRNA in TE7.5 buffer was added, on a drop-by-drop basis, to 800 μL of dichloromethane (DCM) containing 25 mg of PLGA (Corbion, Amsterdam, the Netherlands) and emulsified by sonication into a primary W1/O emulsion. Next, 2 mL of 2% PVA1500 (w/v) was added directly into the primary emulsion and further emulsified by sonication to form a W1/O/W2 double emulsion. The resulting product was then diluted with 6 mL of 2% PVA1500 and stirred magnetically for 3 h at room temperature to evaporate DCM. The resulting PLGA nanoparticles were collected by ultracentrifugation at 38,000 g for 10 min at 4°C, washed twice with deionized RNAase free-water, resuspended in water and finally freeze-dried. (**B**) Nanoparticles were assessed by the scanning electron microscope. Scale bar = 200 nm. (**C, D**) p66shc si_NPs were dissolved in water and measured for size and zeta potential using the Zetasizer Nano ZS90 (Size = 183.7 ± 72.21, Zeta potential = 41.1 ± 4.81). (**E**) siRNA release assay of nanoparticles in PBS showed the cumulative percentages of siRNA released from nanoparticles based on different matrices as a function of time.

Abbreviation: PLGA, poly(lactic-*co*-glycolic acid).

dedicated software. The plates were retained and protein concentrations were calculated to confirm that the wells contained approximately equal numbers of cells.

In vitro Nanoparticles Release Assay

The p66shc siRNA encapsulated PLGA nanoparticles were collected and incubated in Eppendorf tube with 250 μL of PBS, incubated at 37 °C, for 48 h. At the designated time, 200 μL of the release medium was taken and replaced by the same amount of fresh buffer. P66shc siRNA was measured in the release buffer using nanodrop spectrometer (Thermo scientific). The accumulated release percentage of the p66shc siRNA and the entrapment efficiency were evaluated according to previous report.[33]

Statistical Analysis

Data are presented as the means ± SEM. We compared group mean values, as appropriate, by Student's *t*-test or one-way analysis of variance with post hoc multiple comparison test (GraphPad Prism 6). We considered $p < 0.05$ as the significant value.

Results

p-p66shc Is Highly Expressed in Cartilage from OA Patients and MIA-Induced OA Rats

The significance of ROS production during cartilage damage implies a role for p66shc in the pathogenesis of OA. We examined the expression levels of the ROS-production-related proteins p66shc in joint tissues from OA patients using immunohistochemistry. Both phosphorylated p66shc (p-p66shc) was stained in articular cartilage, with especially intense staining observed in superficial chondrocyte clusters (Figure 2A). Chondrocytes clustering is a histological sign of late-stage OA and is particularity evident in the superficial zones of OA patient tissues.[5,34] Over 80% of the clusters expressed p-p66shc at high levels (Figure 2B).

Monosodium iodoacetate (MIA) is used to induce cartilage damage in animal models of OA involving ROS production.[35] Chondrocytes were incubated for 24 h either with or without 1, 5, and 15 μM MIA, and cell viability was measured. Cell viability was approximately 20% in chondrocytes treated with MIA at concentrations >5 μM, and cell viability decreased in a time-dependent manner (Figure 3A). Next, we investigated whether the effects of MIA on chondrocytes were attributable to p66shc phosphorylation and ROS production. In MIA-treated chondrocytes, Western blotting showed that p66shc phosphorylation increased significantly compared with that in control chondrocytes (Figure 2C and D). Thus, MIA induces the phosphorylation of p66shc in human chondrocytes.

Induction of OA by intra-articular injection of MIA into rat knee joints (Suppl Figure 1A) results in the progressive loss of articular cartilage and the development of subchondral bone lesions; these features closely resemble those observed in OA.[36] We used three different doses of MIA to determine whether these effects were dose-dependent (Suppl Figure 1B). On day 3, either no change or only a minimal decrease in proteoglycan levels (as revealed by Safranin-O staining) was observed in animals injected with 0.5 and 1 mg MIA. At the highest dose (2 mg), articular cartilage loss from the extracellular matrix was more pronounced on day 3 (Suppl Figure 1B). Identical results were obtained in the sagittal plane as coronal plane (Suppl Figure 1C). Micro-computed tomography (CT) showed that articular cartilage thickness decreased, hyaline articular cartilage became eroded, and subchondral bone became exposed in a dose- and time-dependent manner (Suppl Figure 1D), similar to the effects observed during human OA.

MIA has also been reported to induce apoptosis via the mitochondrial pathway and involving ROS production in rat chondrocytes.[35] Because cartilage damage caused by MIA might be associated with ROS production, we measured the expression levels of the ROS-associated proteins p-p66shc. By day 3, animals injected with 2 mg MIA exhibited significantly increased expression levels of p-p66shc compared with control animals (Figure 2E and F), suggesting that the upregulation of p-p66shc expression levels in cartilage is associated with articular cartilage loss.

MIA Causes Mitochondrial Dysfunction and ROS Production, and the Inhibition of p66shc Phosphorylation Attenuates MIA-Induced ROS Production in Human Chondrocytes

Next, we assessed whether MIA affected primary human chondrocyte viability. Chondrocytes were incubated for 24 h with or without 1, 5, and 15 μM MIA. As shown in Figure 3A, cell viability was only approximately 20% after treatment with MIA at concentrations >5 μM, and fell in a time-dependent manner (Figure 3B). Thus, human

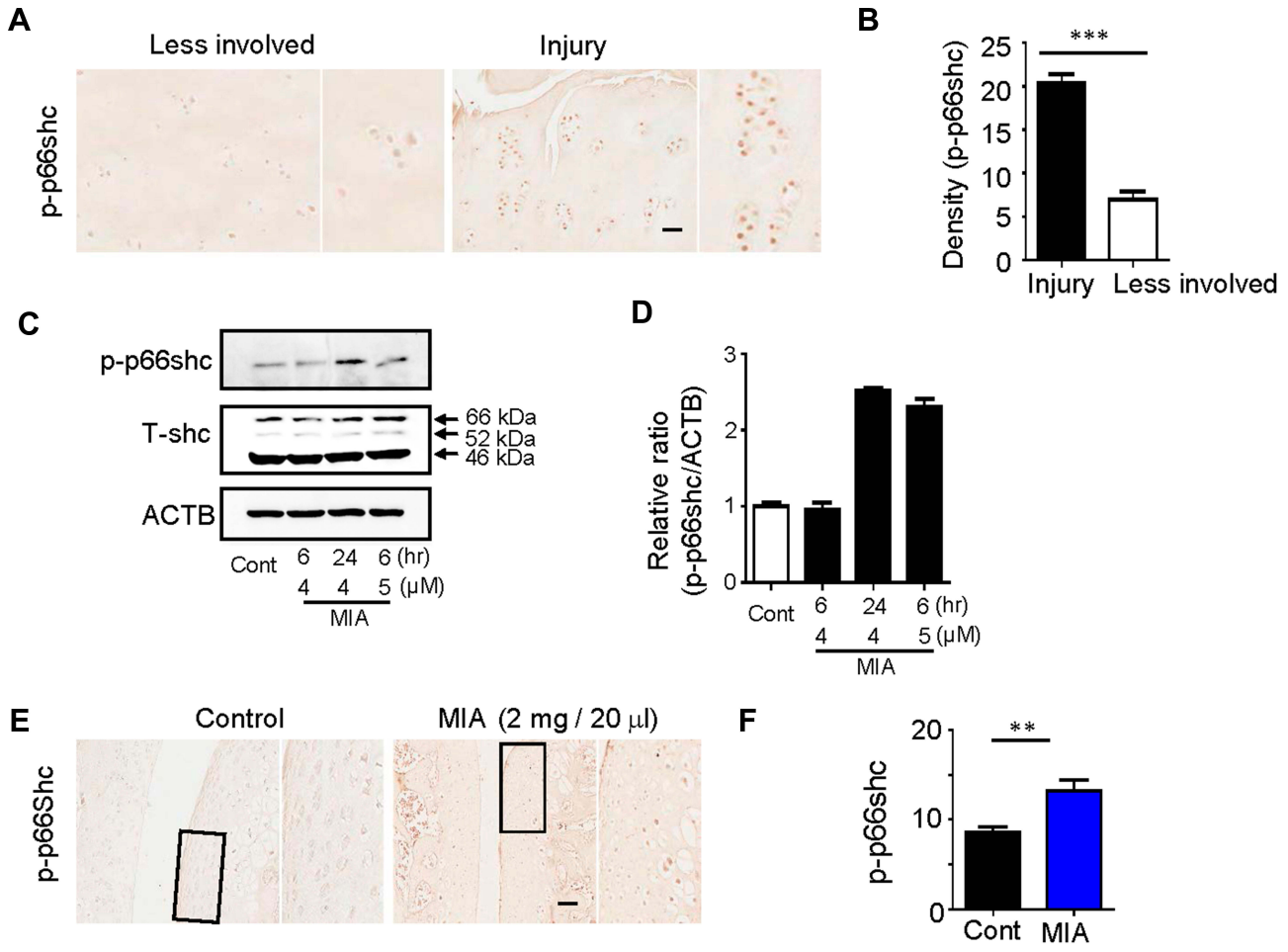

Figure 2 Expression of p66shc in articular cartilage from OA patients and MIA-induced rat models.
Notes: (**A, B**) p-p66shc was prominently expressed at sites of injury. Scale bar = 50 μm. ***$P < 0.001$ (**C, D**) p-p66shc and total shc protein levels were detected via Western blotting, and the p-p66shc/ACTB ratios were determined using Image J software. (**E, F**) Expression levels of p66shc in knee cartilage as measured with immunohistochemical staining. Protein density was quantified using Image J software (NIH, USA). Scale bar = 50 μm. **$P < 0.01$.
Abbreviations: OA, osteoarthritis; MIA, monosodium iodoacetate; ACTB, actin beta.

chondrocyte viability was MIA concentration-dependent, suggesting that MIA can also damage human chondrocytes.

Because mitochondria are the predominant sites for ROS production and the primary targets of ROS, these organelles play a key role in oxidative stress and inflammation and can tip the balance toward functional failure and cell death.[37] To explore whether MIA-induced ROS production initiated mitochondrial dysfunction, primary chondrocyte cells were incubated with MIA, and the basal OCR was determined using an XF-24 analyzer. H_2O_2 triggers oxidative stress and cell death because it readily permeates mitochondria; therefore, H_2O_2 was used as a positive control.[38] In the presence of either H_2O_2 or MIA, cellular oxygen consumption was initially identical to that of controls. However, MIA-treated cells showed decreased maximal mitochondrial OCR capacity after CCCP treatment compared with control cells (Figure 3C). After the state III oxidation rate was reduced, the maximal mitochondrial respiratory chain activity decreased significantly in MIA-treated cells compared with that of control cells. We also measured the ECAR, which is a glycolysis index. MIA-treated cells showed decreased ECAR compared with controls (Figure 3D), which represents the inhibition of cytosolic metabolic flow, demonstrating that MIA induced mitochondrial dysfunction in human chondrocytes.

Since p66shc is involved in ROS production, we investigated the effect of p66shc inhibition on MIA-treated chondrocytes. ROS production was quantitated using the mitoSOX fluorescence assay in MIA-treated chondrocytes treated with or without a recombinant

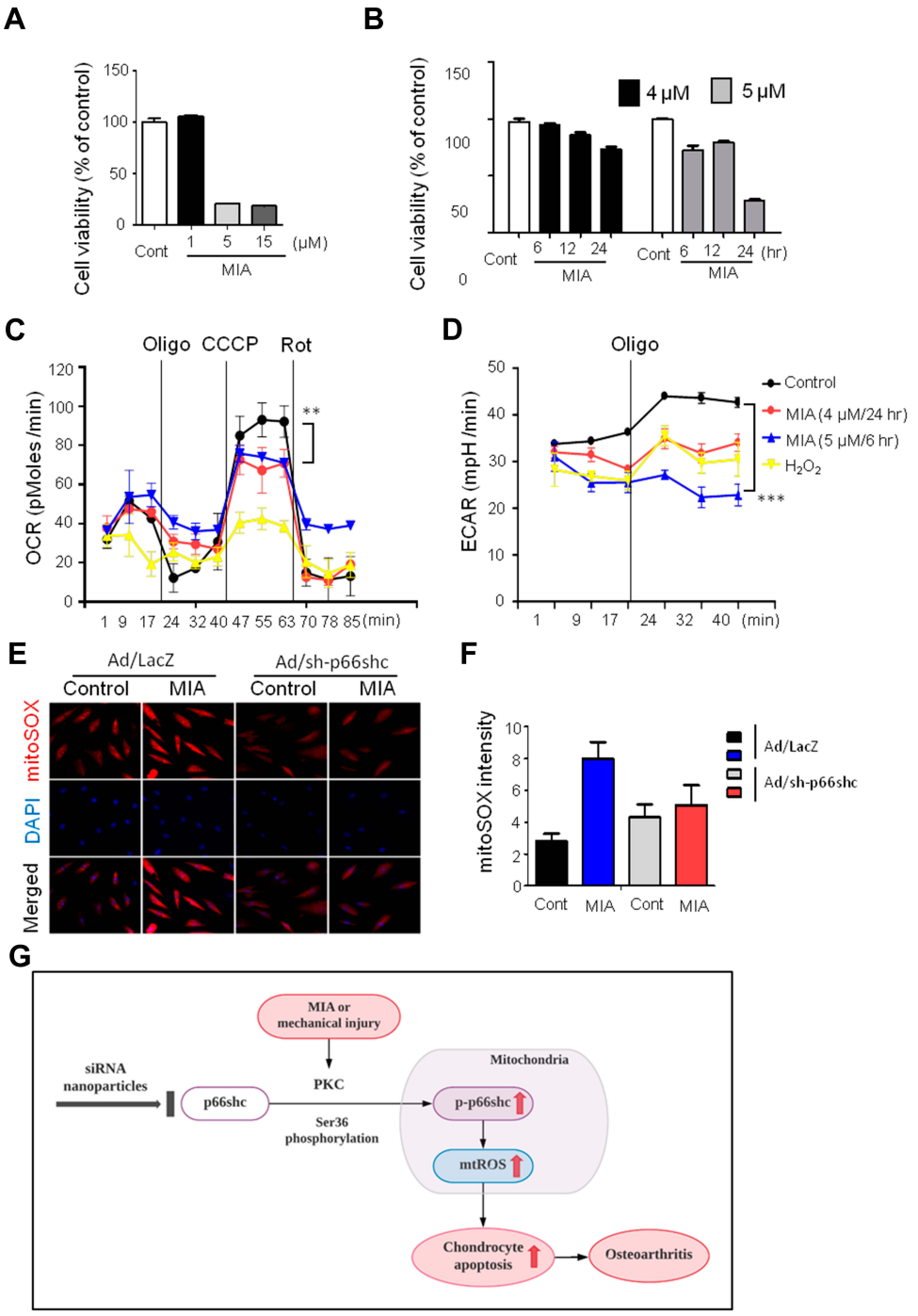

Figure 3 MIA caused mitochondrial dysfunction and ROS production, and inhibition of p66shc alleviated MIA-induced mtROS production in human chondrocytes.
Notes: (**A, B**) Extent of cytotoxicity following MIA treatment, according to time and dose. (**C, D**) The oxygen consumption rate (OCR), which reflects mitochondrial function, and the extracellular acidification rate (ECAR), which indicates lactate production, were obtained using a Seahorse XF24 analyzer in cells treated with 2 μg/mL oligomycin (an ATPase inhibitor), 5 μM cyanide m-chlorophenylhydrazone (CCCP; an uncoupler), or 2 μM rotenone (a mitochondrial complex I inhibitor). Area under the curve (AUC) for basal OCR and ECAR were measured from the first to the third timepoints. The AUC for maximal OCR was measured from the seventh to the ninth timepoints. Data represent the mean ± SEM (error bars) of three experiments. $^{**}P < 0.01$, $^{***}P < 0.001$ (derived via one-way ANOVA); MIA vs control. (**E**) MitoSOX fluorescence imaging of human chondrocytes expressing Ad/LacZ and Ad/sh-p66shc. (**F**) Quantification of MitoSOX fluorescence. (**G**) Schematic diagram of p66shc-related pathway.
Abbreviation: ROS, reactive oxygen species.

adenovirus encoding an shRNA targeting p66shc (Ad/sh-p66shc). MitoSOX fluorescence intensity greatly increased in MIA-treated cells, and the intensity was inhibited by downregulation of p66shc with Ad/sh-p66shc (Figure 3E and F). Thus, downregulation of p66shc attenuated MIA-induced ROS production in

human chondrocytes (Figure 3G). These results suggest that p66shc may be related to human OA.

Inhibition of p66shc by Nanoparticles-Delivered siRNA Ameliorates Pain Behavior, Cartilage Damage, and Inflammation in the Knee Joints of MIA-Induced OA Rats

Next, we explored the therapeutic potential of p66shc siRNA in the MIA-induced OA model. For the efficient delivery of p66shc siRNA into joints, we used poly(lactic-*co*-glycolic acid) PLGA copolymers, which are biodegradable and biocompatible with humans, and have been approved by the FDA.[39] p66shc-siRNA-loaded PLGA NPs (p66shc si_PLGA NPs) were prepared by sonication, using the double emulsion (water-in-oil-in-water [W/O/W]) method to encapsulate hydrophilic siRNA (Figure 1A). The scanning electron microscopy showed that the particles were spheroids (Figure 1B). The average size and zeta potential were 183.7.8 ± 72.21 nm and 41.1 ± 4.81 mV, respectively (Figure 1C and D). siRNA release assay of nanoparticles at pH 7.4 was conducted in a PBS buffer, as the model of biological body fluids. It was found from the Figure 1E that the cumulative siRNA release of 96.4% was within 48 hr.

Subsequently, we delivered the single-dose PLGA NPs containing 0.2 μmol/20μL of either p66shc siRNA or scrambled siRNA into the each knee joint of MIA-treated rats (Figure 4A), and the rats were subjected to the von Frey filament test and CatWalk analysis. Injection of 20 μL MIA (2 mg) induced mechanical allodynia of the ipsilateral paw compared with saline-treated controls. However, injection of p66shc si_PLGA NP alleviated mechanical allodynia in rats treated with MIA for up to 21 days after MIA injection (Figure 4B). The print area is the surface area of a complete print, and the standing phase is the duration of paw contact with the glass plate (in seconds). The print areas of the ipsilateral paws of MIA-injected rats were reduced, but they recovered after p66shc si_PLGA NP injection (Figure 4C); a similar result was observed for the standing phase duration of the ipsilateral paw (Figure 4D). We also compared the pathological changes in MIA-injected joints between animals treated with p66shc si_PLGA NPs and those treated with control NPs. Safranin-O stain showed that p66shc si_PLGA NPs attenuated proteoglycan loss 3 weeks after MIA injection (Figure 4E). Cartilage thickness and the number of chondrocytes were also reduced after MIA injection in animals that received control NP injections. However, these pathologies were attenuated by the p66shc si_PLGA NP injections (Figure 4E and F). In addition, micro-CT revealed that destruction of the bony surface was attenuated by p66shc si_PLGA NP injections at weeks 2 and 4 (Figure 4G).

MIA has recently been known to evoke acute inflammation, followed by degenerative cartilage changes and joint pain.[40] Therefore, we explored whether MIA injections induced an inflammatory response that could be reversed by p66shc si_PLGA NPs. MIA clearly increased the expression levels of inflammatory genes, including those encoding tumor necrosis factor (TNF)-α, interleukin (IL)-1β, and cyclooxygenase 2 (COX2) (Figure 4H–J). However, the expression levels of all inflammatory cytokines were markedly decreased in the p66shc si_PLGA NP group. Together, these findings suggest that p66shc inhibition attenuates pain behaviors, cartilage damage and the expression of inflammatory cytokines in the arthritic knee joints of MIA-induced animal models.

Discussion

Here, we investigated the involvement of p66shc during cartilage degeneration in OA. A role for p66shc during cartilage degeneration was suggested by the immunohistochemical analysis of tissues from OA patients. Moreover, p66shc-mediated ROS production triggered mitochondrial dysfunction in human chondrocytes, which was prevented by the application of an adenoviral vector encoding shRNA-p66shc. Finally, by injecting p66shc-RNAi-loaded NPs into the knee joints of rats with MIA-induced OA, we investigated the therapeutic potential of p66shc inhibition in OA. We used an MIA-induced cartilage damage model, which induces rapid pain-like responses in the cartilage and has become the standard for exploring OA-mediated joint disruption in both rats and mice. The morphological changes observed in articular cartilage and bone resemble those observed during human OA.[36] Although traumatic OA models, induced by meniscus or anterior cruciate ligament resection, are also commonly used, the MIA model is more appropriate for exploring the changes caused by mitochondrial pathology and ROS production. In addition, we found that the evoked pain persisted significantly after MIA administration.

p66shc plays a key role in the oxidative stress related to kidney, cardiovascular, and lung disease.[16–19] *p66shc* deletion ($p66shc^{-/-}$) in mice is associated with resistance to oxidative stress and a reduction in p53-dependent apoptosis. $p66shc^{-/-}$ mice do not develop emphysema after

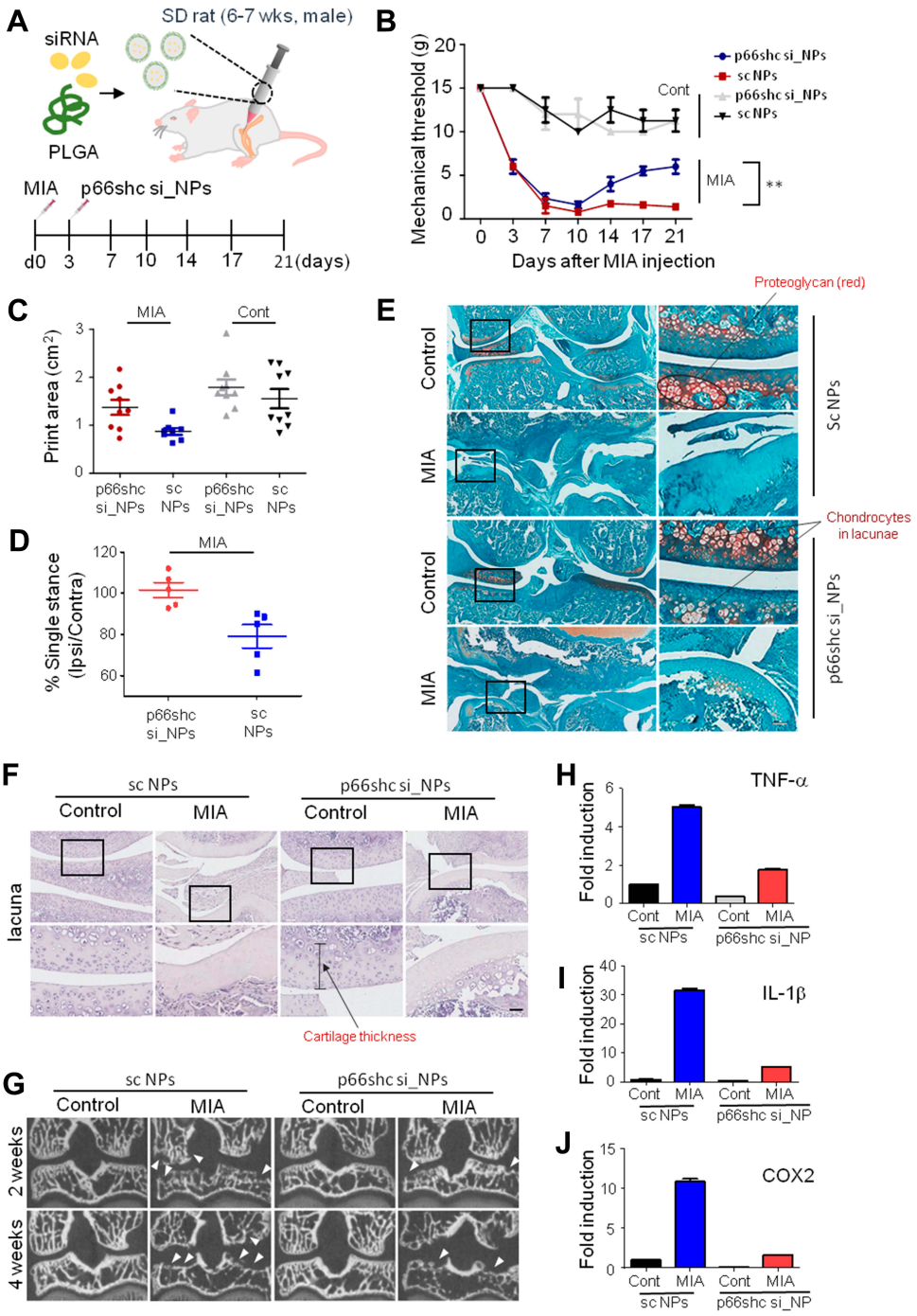

Figure 4 P66shc deficiency attenuates pain behavior, cartilage damage, and inflammation in MIA-induced OA animal model knee joints.

Notes: (**A**) Schematic of protocol for injecting p66shc siRNA encapsulated in poly(lactic-*co*-glycolic acid) (PLGA) nanoparticles (NPs) (p66shc si_PLGA NPs) into rats with MIA-induced OA. PLGA NPs containing scrambled siRNA or p66shc si_PLGA NPs were delivered to the knee using a Hamilton syringe. (**B**) Rats were subjected to behavioral testing using Von Frey filaments (n = 7–8 per group). $^{**}P < 0.01$ (**C**) Paw print areas of the legs with MIA-injected knees, as assessed by CatWalk analysis. (**D**) The percentage (ipsi-/contra-lateral single standing) of ipsilateral paw single standing was measured in MIA-injected rats treated with p66shc si_PLGA NPs. (**E**) Safranin-O and Fast Green staining of knee joints from rats treated with MIA for 3 weeks. (Scale bar = 50 μm) The intensity of Safranin O staining is proportional to the proteoglycan content in the cartilage tissue. (**F**) Hematoxylin staining of paraffin-embedded sections of the knee joint. (Scale bar = 50 μm) (**G**) Representative transverse CT images of tibial subchondral bony destruction (arrowheads) at 3 weeks after injection with p66shc si_PLGA NPs. (**H–J**) Expression levels of tumor necrosis factor (TNF)-α (**H**), interleukin (IL)-1β (**I**), and cyclooxygenase 2 (COX2) (**J**) by qRT-PCR. Total mRNA was isolated from rat knee cartilage. Scale bar = 50 μm.

Abbreviations: PLGA, poly(lactic-*co*-glycolic acid); NPs, nanoparticles.

chronic exposure to smoke,[41] and *p66shc* deficiency prolongs lifespan, decreasing cytoplasmic ROS levels by activating NADPH oxidase (Nox). However, later studies found that p66shc was also present in mitochondria and bound to cytochrome C to form H_2O_2.[42] Mitochondrial p66shc levels are increased by protein kinase Cβ (PKCβ), and ROS induced by p66shc are involved in p53-mediated apoptosis, ischemic heart disease, and autoimmune suppression. Recent studies have shown that p66shc phosphorylates Rac1, an enzyme that interacts with Nox in vascular endothelial cells, resulting in increased ROS levels.[43] However, p66shc disrupts mitochondrial function via its CYCS (cytochrome c, somatic) binding domain, impairing ATP production, activating AMP-activated protein kinase (AMPK) and enhancing autophagic flux.[44]

ROS are generated by the Nox family of enzyme complexes, which catalyze the transfer of electrons from NADPH to molecular oxygen, generating O_2.[45,46] Thus, p66Shc deficiency reduced the activation of the PHOX complex, decreasing superoxide production.[47] Because mitochondrial dysfunction is induced by oxidative damage, correlations between the levels of oxidative damage and the levels of p66shc and Nox protein expression should be examined in OA experimental models.

p66shc mediates oxidative stress in aging and cardiovascular diseases, but the role played by this protein in musculoskeletal disorders remains unclear. Few studies have evaluated the pathogenic effects of p66shc after mtROS generation. This study is the first to reveal the role played by p66shc in articular cartilage degeneration. We explored whether OA was associated with p66shc-mediated mitochondrial dysfunction, and revealed that excessive oxidative stress induces cartilage destruction via p66shc phosphorylation.

Furthermore, we applied siRNA PLGA NPs that inhibited p66shc phosphorylation-induced ROS production, mitochondrial dysfunction and, ultimately, cartilage degeneration. The double emulsion process (water-in-oil-in-water) was used in our experiment, and the inner core of water was for encapsulating hydrophilic siRNA. In in-vivo application, release duration may be shorter than 48 hr in our in-vitro experiment with a PBS buffer.[48] After siRNA is released from nanoparticles, there can be several barriers such as cleavage by enzymes in serum or cytoplasm. Although there can be less obstacles for intra-articular delivery in the knee joint, further investigation about siRNA modification will be needed to ensure gene silencing efficacy.

In conclusion, we first investigated the involvement of p66shc during cartilage degeneration in OA. By injecting p66shc-RNAi-loaded NPs into the knee joints of rats with MIA-induced OA, mitochondrial dysfunction-induced cartilage damage was significantly decreased. Therefore, we expect p66shc siRNA PLGA nanoparticles represent a promising novel therapy for OA.

Abbreviations

OA, osteoarthritis; MIA, monosodium iodoacetate; ROS, reactive oxygen species; PLGA, poly(lactic-*co*-glycolic acid); NPs, nanoparticles; qPCR, quantitative polymerase chain reaction; OCR, oxygen consumption rate; ECAR, extracellular acidification rate; CCCP, carbonyl cyanide m-chlorophenylhydrazone; SEM, standard error of mean; micro-CT, micro-computed tomography; TNF-α, tumor necrosis factor-α; IL-1β, interleukin-1β; COX2, cyclooxygenase 2; ACTB, actin beta.

Acknowledgments

This research was supported by the Brain Research Program through the National Research Foundation of Korea (NRF) funded by the Ministry of Science, ICT & Future Planning (NRF-2016R1A2B4009409 and NRF-2017R1A5A2015385), and the Basic Science Research Program through the NRF funded by the Ministry of Education (NRF-2018R1D1A1B07043681 and NRF-2016R1D1A1B03933919).

Disclosure

The authors report no conflicts of interest in this work.

References

1. Ziskoven C, Jager M, Zilkens C, Bloch W, Brixius K, Krauspe R. Oxidative stress in secondary osteoarthritis: from cartilage destruction to clinical presentation? *Orthop Rev (Pavia)*. 2010;2(2):e23. doi:10.4081/or.2010.e23
2. Lee CM, Kisiday JD, McIlwraith CW, Grodzinsky AJ, Frisbie DD. Synoviocytes protect cartilage from the effects of injury in vitro. *BMC Musculoskelet Disord*. 2013;14:54. doi:10.1186/1471-2474-14-54
3. Sandell LJ, Aigner T. Articular cartilage and changes in arthritis. An introduction: cell biology of osteoarthritis. *Arthritis Res*. 2001;3(2):107–113. doi:10.1186/ar148
4. Khan IM, Palmer EA, Archer CW. Fibroblast growth factor-2 induced chondrocyte cluster formation in experimentally wounded articular cartilage is blocked by soluble Jagged-1. *Osteoarthritis Cartilage*. 2010;18(2):208–219. doi:10.1016/j.joca.2009.08.011
5. Hoshiyama Y, Otsuki S, Oda S, et al. Chondrocyte clusters adjacent to sites of cartilage degeneration have characteristics of progenitor cells. *J Orthop Res*. 2015;33(4):548–555. doi:10.1002/jor.v33.4
6. Del Carlo M Jr., Loeser RF. Nitric oxide-mediated chondrocyte cell death requires the generation of additional reactive oxygen species. *Arthritis Rheum*. 2002;46(2):394–403.

7. Horton WE Jr., Feng L, Adams C. Chondrocyte apoptosis in development, aging and disease. *Matrix Biol*. 1998;17(2):107–115. doi:10.1016/S0945-053X(98)90024-5
8. Soto-Hermida A, Fernandez-Moreno M, Pertega-Diaz S, et al. Mitochondrial DNA haplogroups modulate the radiographic progression of Spanish patients with osteoarthritis. *Rheumatol Int*. 2015;35 (2):337–344. doi:10.1007/s00296-014-3104-1
9. Liu JT, Guo X, Ma WJ, et al. Mitochondrial function is altered in articular chondrocytes of an endemic osteoarthritis, Kashin-Beck disease. *Osteoarthritis Cartilage*. 2010;18(9):1218–1226. doi:10.1016/j.joca.2010.07.003
10. Fernandez-Moreno M, Soto-Hermida A, Pertega S, et al. Mitochondrial DNA (mtDNA) haplogroups and serum levels of anti-oxidant enzymes in patients with osteoarthritis. *BMC Musculoskelet Disord*. 2011;12:264. doi:10.1186/1471-2474-12-264
11. Lee SW, Song YS, Shin SH, et al. Cilostazol protects rat chondrocytes against nitric oxide-induced apoptosis in vitro and prevents cartilage destruction in a rat model of osteoarthritis. *Arthritis Rheum*. 2008;58(3):790–800.
12. Lebiedzinska M, Karkucinska-Wieckowska A, Giorgi C, et al. Oxidative stress-dependent p66Shc phosphorylation in skin fibroblasts of children with mitochondrial disorders. *Biochim Biophys Acta*. 2010;1797(6):952–960. doi:10.1016/j.bbabio.2010.03.005
13. Galimov ER. The role of p66shc in oxidative stress and apoptosis. *Acta Naturae*. 2010;2(4):44–51. doi:10.32607/20758251-2010-2-4-44-51
14. Bhat SS, Anand D, Khanday FA. p66Shc as a switch in bringing about contrasting responses in cell growth: implications on cell proliferation and apoptosis. *Mol Cancer*. 2015;14.
15. Khanday FA, Yamamori T, Mattagajasingh I, et al. Rac1 leads to phosphorylation-dependent increase in stability of the p66shc adaptor protein: role in Rac1-induced oxidative stress. *Mol Biol Cell*. 2006;17 (1):122–129. doi:10.1091/mbc.e05-06-0570
16. Menini S, Iacobini C, Ricci C, et al. Ablation of the gene encoding p66Shc protects mice against AGE-induced glomerulopathy by preventing oxidant-dependent tissue injury and further AGE accumulation. *Diabetologia*. 2007;50(9):1997–2007. doi:10.1007/s00125-007-0728-7
17. Nagar H, Jung SB, Kwon SK, et al. CRIF1 deficiency induces p66shc-mediated oxidative stress and endothelial activation. *PLoS One*. 2014;9(6):e98670. doi:10.1371/journal.pone.0098670
18. Yang M, Stowe DF, Udoh KB, Heisner JS, Camara AK. Reversible blockade of complex I or inhibition of PKCbeta reduces activation and mitochondria translocation of p66Shc to preserve cardiac function after ischemia. *PLoS One*. 2014;9(12):e113534. doi:10.1371/journal.pone.0113534
19. Ziolkowski W, Flis DJ, Halon M, et al. Prolonged swimming promotes cellular oxidative stress and p66Shc phosphorylation, but does not induce oxidative stress in mitochondria in the rat heart. *Free Radic Res*. 2015;49(1):7–16. doi:10.3109/10715762.2014.968147
20. Blanco FJ, Lopez-Armada MJ, Maneiro E. Mitochondrial dysfunction in osteoarthritis. *Mitochondrion*. 2004;4(5–6):715–728. doi:10.1016/j.mito.2004.07.022
21. Malik A, Gupta M, Mani R, Bhatnagar R. Single-dose Ag85B-ESAT6-loaded poly(lactic-co-glycolic acid) nanoparticles confer protective immunity against tuberculosis. *Int J Nanomedicine*. 2019;14: 3129–3143. doi:10.2147/IJN.S172391
22. Te Boekhorst BC, Jensen LB, Colombo S, et al. MRI-assessed therapeutic effects of locally administered PLGA nanoparticles loaded with anti-inflammatory siRNA in a murine arthritis model. *J Control Release*. 2012;161(3):772–780. doi:10.1016/j.jconrel.2012.05.004.
23. Maji R, Dey NS, Satapathy BS, Mukherjee B, Mondal S. Preparation and characterization of Tamoxifen citrate loaded nanoparticles for breast cancer therapy. *Int J Nanomedicine*. 2014;9:3107–3118. doi:10.2147/IJN.S63535
24. Ben David-Naim M, Grad E, Aizik G, et al. Polymeric nanoparticles of siRNA prepared by a double-emulsion solvent-diffusion technique: physicochemical properties, toxicity, biodistribution and efficacy in a mammary carcinoma mice model. *Biomaterials*. 2017;145:154–167. doi:10.1016/j.biomaterials.2017.08.036
25. Ramot Y, Rotkopf S, Gabai RM, et al. Preclinical safety evaluation in rats of a polymeric matrix containing an siRNA drug used as a local and prolonged delivery system for pancreatic cancer therapy. *Toxicol Pathol*. 2016;44(6):856–865. doi:10.1177/0192623316645860
26. Kapoor DN, Bhatia A, Kaur R, Sharma R, Kaur G, Dhawan S. PLGA: a unique polymer for drug delivery. *Ther Deliv*. 2015;6 (1):41–58. doi:10.4155/tde.14.91
27. Sadat Tabatabaei Mirakabad F, Nejati-Koshki K, Akbarzadeh A, et al. PLGA-based nanoparticles as cancer drug delivery systems. *Asian Pac J Cancer Prev*. 2014;15(2):517–535. doi:10.7314/APJCP.2014.15.2.517.
28. Johnson RH, Hu H, Haworth ST, Cho PS, Dawson CA, Linehan JH. Feldkamp and circle-and-line cone-beam reconstruction for 3D micro-CT of vascular networks. *Phys Med Biol*. 1998;43 (4):929–940. doi:10.1088/0031-9155/43/4/020
29. Bakker B, Eijkel GB, Heeren RM, Karperien M, Post JN, Cillero-Pastor B. Oxygen regulates lipid profiles in human primary chondrocyte cultures. *Osteoarthr Cartil*. 2016;24:S456–S457. doi:10.1016/j.joca.2016.01.833
30. Roh DH, Kim HW, Yoon SY, et al. Intrathecal injection of the sigma (1) receptor antagonist BD1047 blocks both mechanical allodynia and increases in spinal NR1 expression during the induction phase of rodent neuropathic pain. *Anesthesiology*. 2008;109(5):879–889. doi:10.1097/ALN.0b013e3181895a83
31. Zhang E, Yi MH, Shin N, et al. Endoplasmic reticulum stress impairment in the spinal dorsal horn of a neuropathic pain model. *Sci Rep*. 2015;5:11555. doi:10.1038/srep11555
32. Shin J, Yin Y, Park H, et al. p38 siRNA-encapsulated PLGA nanoparticles alleviate neuropathic pain behavior in rats by inhibiting microglia activation. *Nanomedicine (Lond)*. 2018;13(13):1607–1621. doi:10.2217/nnm-2018-0054
33. Peltonen L, Aitta J, Hyvonen S, Karjalainen M, Hirvonen J. Improved entrapment efficiency of hydrophilic drug substance during nanoprecipitation of poly(l)lactide nanoparticles. *AAPS PharmSciTech*. 2004;5:1.
34. Karim A, Amin AK, Hall AC. The clustering and morphology of chondrocytes in normal and mildly degenerate human femoral head cartilage studied by confocal laser scanning microscopy. *J Anat*. 2018;232(4):686–698. doi:10.1111/joa.2018.232.issue-4
35. Jiang LP, Li LJ, Geng CY, et al. Monosodium iodoacetate induces apoptosis via the mitochondrial pathway involving ROS production and caspase activation in rat chondrocytes in vitro. *J Orthop Res*. 2013;31(3):364–369. doi:10.1002/jor.v31.3
36. Pitcher T, Sousa-Valente J, Malcangio M. The monoiodoacetate model of osteoarthritis pain in the mouse. *J Vis Exp*. 2016;111.
37. Maneiro E, Lopez-Armada MJ, de Andres MC, et al. Effect of nitric oxide on mitochondrial respiratory activity of human articular chondrocytes. *Ann Rheum Dis*. 2005;64(3):388–395. doi:10.1136/ard.2004.022152
38. Chernyak BV, Izyumov DS, Lyamzaev KG, et al. Production of reactive oxygen species in mitochondria of HeLa cells under oxidative stress. *Biochim Biophys Acta*. 2006;1757(5):525–534. doi:10.1016/j.bbabio.2006.02.019
39. Menon JU, Kuriakose A, Iyer R, et al. Dual-drug containing core-shell nanoparticles for lung cancer therapy. *Sci Rep*. 2017;7 (1):13249. doi:10.1038/s41598-017-13320-4
40. Moilanen LJ, Hamalainen M, Nummenmaa E, et al. Mia-induced inflammation and joint pain are reduced in Trpa1 deficient mice - potential role for Trpa1 in osteoarthritis. *Osteoarthr Cartil*. 2015;23: A259–A259. doi:10.1016/j.joca.2015.02.472

41. Lunghi B, De Cunto G, Cavarra E, et al. Smoking p66Shc knocked out mice develop respiratory bronchiolitis with fibrosis but not emphysema. *PLoS One*. 2015;10(3):e0119797. doi:10.1371/journal.pone.0119797
42. Giorgio M, Migliaccio E, Orsini F, et al. Electron transfer between cytochrome c and p66Shc generates reactive oxygen species that trigger mitochondrial apoptosis. *Cell*. 2005;122(2):221–233. doi:10.1016/j.cell.2005.05.011
43. Oshikawa J, Kim SJ, Furuta E, et al. Novel role of p66Shc in ROS-dependent VEGF signaling and angiogenesis in endothelial cells. *Am J Physiol Heart Circ Physiol*. 2012;302(3):H724–732. doi:10.1152/ajpheart.00739.2011
44. Onnis A, Cianfanelli V, Cassioli C, et al. The pro-oxidant adaptor p66SHC promotes B cell mitophagy by disrupting mitochondrial integrity and recruiting LC3-II. *Autophagy*. 2018;14(12):2117–2138. doi:10.1080/15548627.2018.1505153
45. De Marchi E, Baldassari F, Bononi A, Wieckowski MR, Pinton P. Oxidative stress in cardiovascular diseases and obesity: role of p66Shc and protein kinase C. *Oxid Med Cell Longev*. 2013;2013:564961. doi:10.1155/2013/564961
46. Ma W, Li J, Hu J, et al. miR214-regulated p53-NOX4/p66shc pathway plays a crucial role in the protective effect of Ginkgolide B against cisplatin-induced cytotoxicity in HEI-OC1 cells. *Chem Biol Interact*. 2016;245:72–81.
47. Tomilov AA, Bicocca V, Schoenfeld RA, et al. Decreased superoxide production in macrophages of long-lived p66Shc knock-out mice. *J Biol Chem*. 2010;285(2):1153–1165. doi:10.1074/jbc.M109.017491
48. Rafiei P, Haddadi A. Docetaxel-loaded PLGA and PLGA-PEG nanoparticles for intravenous application: pharmacokinetics and biodistribution profile. *Int J Nanomedicine*. 2017;12:935–947. doi:10.2147/IJN.S121881